Appl. Phys. B 63, 255–264 (1996)

Applied Physics B Lasers and Optics

Femtosecond phase spectroscopy of multi-level systems: Phthalocyanines

E. Tokunaga[1,*], A. Terasaki[1,], V. S. Valencia[2,***], T. Wada[2], H. Sasabe[2], T. Kobayashi[1,†]**

[1] Department of Physics, Faculty of Science, University of Tokyo, 7-3-1 Hongo, Bunkyo, Tokyo 113, Japan
(Fax: + 81-3-3818-7812)
[2] Frontier Research Program, The Institute of Physical and Chemical Research (RIKEN), 2-1 Hirosawa, Wako, Saitama 351-01, Japan

Received: 10 October 1995/Accepted: 7 March 1996

Abstract. A femtosecond frequency-domain interferometer is applied to metal-free and vanadyl phthalocyanine (H_2Pc and VOPc) thin films to measure time-resolved difference phase and transmission spectra simultaneously. For both samples, the phase-change dynamics is different from the transmission-change dynamics at 620 nm, reflecting that the phthalocyanines (Pc) cannot be modeled with a two-level system but by a multi-level or inhomogeneously broadened system, in which each level pair exhibits different relaxation dynamics. Because of this dynamical difference, a phase-change measurement is required to correct distortion of the transient spectra due to induced phase modulation of probe pulses. Near zero time delay, the phase and transmission changes show different growth behavior. This behavior is explained by antisymmetric amplitude and phase gratings which are produced by coherent coupling between frequency-chirped pump and probe pulses.

PACS: 07.60.Ly; 42.65.Re; 78.47. + p

We have developed a femtosecond Frequency-Domain Interferometer (FDI) [1] which allows easy access to femtosecond time-resolved dispersion relations [2] in nonlinear optical materials. Previously the FDI was demonstrated using CdS_xSe_{1-x}-doped glass (commercial Toshiba R63 filter) and Kerr liquid CS_2 because of their large nonlinearities and well-established dynamics and mechanisms. For the R63 filter, the observed transmission and phase change showed the same dynamics, which can be explained with a two-level model. For CS_2, only the phase change was observed as expected in a non-resonant probe region. Because of such simple behavior, these samples were suited to demonstrate the feasibility of femtosecond phase spectroscopy and the observed time-resolved spectra were unambiguously reproduced by the simple numerical simulations [3, 4]. In this paper, we extend the application of femtosecond phase spectroscopy to more complex systems, metal-free phthalocyanine (H_2Pc) and vanadyl phthalocyanine (VOPc), which exhibit the dynamics characteristic of multi-level systems or inhomogeneously broadened systems.

Phthalocyanines (Pcs) [5] are synthetic in origin, but structurally similar to the much studied and biologically important porphyrins [6]. Both porphyrins and Pcs have large π-conjugated rings which can incorporate metal ions at their center, exhibiting a large variety of physical and chemical properties [5, 6]. Pcs receive much attention in the field of nonlinear optics because of their relatively large third-order nonlinearity [7–11], which is comparable to that of polydiacetylenes. In our previous studies [7], we have determined the nonlinear optical susceptibilities for Third-Harmonic Generation (THG) in various metallophthalocyanine films (VO-, Sn-, Co-, Ni-, and H_2Pc).

Femtosecond pump–probe and degenerate four-wave mixing measurements have been performed by several groups [12–17] to study the excited-state dynamics for the purpose of elucidating the origin of the nonlinearity. These studies indicate that Pcs exhibit excited-state absorption and excitation-density dependent decay. In addition, our previous studies on various phases of VOPc by femtosecond pump–probe spectroscopy indicate that the excited-state dynamics are strongly dependent on molecular arrangement [17]. However, the previous experiments measured only $\mathrm{Im}\,\chi^{(3)}$ or $|\chi^{(3)}|^2$, where $\chi^{(3)}$ is a third-order nonlinear susceptibility. Here we use the FDI to measure the spectrally resolved femtosecond dynamics of both real and imaginary parts of $\chi^{(3)}$ in phthalocyanines.

Using Pc samples, in Sect. 3 we show that dynamics is different between phase and absorption changes in a multi-level system or an inhomogeneously broadened system. In Sect. 4, we demonstrate that the transient spectra are significantly distorted by the induced modulation effects of probe pulses [18], which cannot be corrected

* *Present address*: Institute for Solid State Physics, University of Tokyo, 7-22-1 Roppongi, Minato-ku, Tokyo 106, Japan
** *Present address*: Department of Chemistry, Faculty of Science, University of Tokyo, 7-3-1 Hongo, Bunkyo-ku, Tokyo 113, Japan
***Formerly* V. S. Williams; *Currently at*: Sandia National Laboratories, P.O. Box 5800, Albuquerque, NM 87185-0338, USA
† To whom all correspondence should be addressed

without a direct phase-change measurement since the Kramers-Kronig relations do not hold in such a case [2, 3]. In Sect. 5, we show that if the pump and probe pulses are chirped, coherent coupling effects lead to different growth dynamics near zero delay between phase and transmission change dynamics.

1 Samples

The polycrystalline thin films of H_2Pc and VOPc were grown by vapor-phase deposition on fused silica substrates at a vapor pressure of ca. 10^{-6} Torr [8]. The absorption spectra for the thin films thus obtained are shown in Fig. 1. The H_2Pc and VOPc films are ca. 0.12 and 0.16 μm thick, respectively, and are comprised of various phases of different molecular stacking configurations [19–21]. The two main absorption peaks, the Q band in the visible and the B band in the ultraviolet, are attributed to the lowest and the second lowest allowed π–π^* transitions in the Pc molecule, that is, the $a_{1u} \rightarrow e_g$ and $a_{2u} \rightarrow e_g$ transitions, respectively. In the solid phase, the twofold degenerate perpendicularly polarized Q band of the VOPc molecule with a C_{4v} symmetry splits due to dimerization by the excitonic interaction [22]. For the D_{2h}-symmetry H_2Pc molecule, the twofold degeneracy of the first π–π^* transition is removed by the lower symmetry of the molecule, resulting in a double-peaked Q band. In the thin film, the double Q band of H_2Pc broadens and blue-shifts with respect to the monomer [23]. We compare the nonlinearities caused by resonant and off-resonant excitation of the Q bands in the H_2Pc and VOPc thin films, respectively. To keep the comparison as objective as possible, the two films were grown to have the same optical density at the excitation wavelength, 620 nm.

2 Experimental

The experimental apparatus is depicted elsewhere [1, 3, 17]. For both excitation and probing, 10 kHz, 60 fs pulses at 620 nm were used. The average pump power was reduced to lower than the damage threshold of the samples, 1 mW. The excitation energy density, power density, and photon density were 5.1×10^{-3} J/cm^2, 8.5×10^{10} W/cm^2, and 1.6×10^{16}/cm^2, respectively. The polarization of the pump and probe pulses was parallel if not specifically noted and all the femtosecond experiments were performed at room temperature. By blocking the reference beams in the FDI and using lock-in detection, standard pump–probe measurements were performed on both thin films. In the FDI measurements, transient spectra with and without excitation were taken alternately with a mechanical shutter operated at 5 Hz.

3 Results and discussion

3.1 Results

Figure 2a and b shows the decay curves of the transmission change $\Delta T(\tau)$ in H_2Pc and VOPc, respectively, as

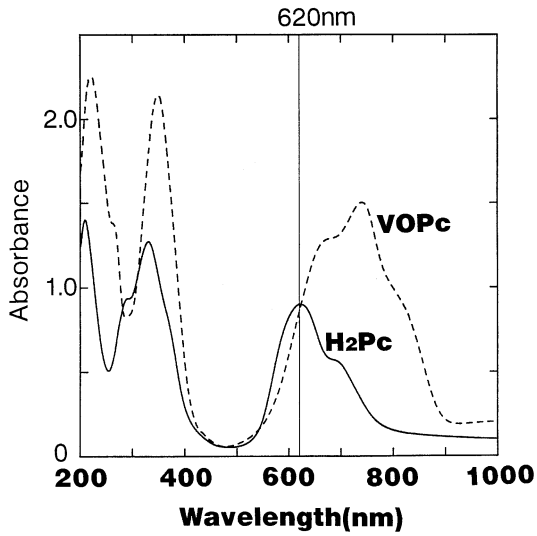

Fig. 1. Absorption spectra of 0.12 μm thick H_2Pc film (*solid line*) and 0.16 μm thick VOPc film (*dashed line*). The vertical line denotes the pump–probe peak wavelength, 620 nm

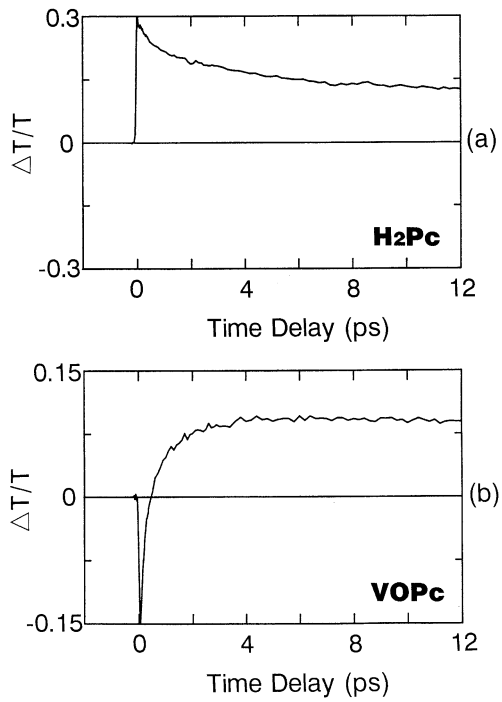

Fig. 2a, b. Delay-time dependence of transmission changes, $\Delta T/T(\tau)$, at 620 nm for (**a**) H_2Pc and (**b**) VOPc by pump–probe measurements with lock-in detection. Vertical scales are estimated from calibration

a function of time delay τ between the pump and probe pulses. H_2Pc exhibits a rapid bleaching signal at 620 nm which then decays on a slower time scale, while VOPc initially exhibits rapid induced absorption which evolves into a bleaching signal after about 400 fs.

Femtosecond interference data were then taken using the FDI [1, 3]. The time-resolved transmission-change spectra, $\Delta T/T(\omega, \tau)$, and phase-change spectra, $\Delta\Phi(\omega, \tau)$,

in H_2Pc and VOPc are shown in Figs. 3 and 4, respectively. Here, ω is the probe frequency and the spectra are measured as a function of wavelength. The reference and probe pulses were temporally displaced by 620 fs so that data could be obtained up to 500 fs delay times without pump pulse influence on the reference pulse. The systematic errors in $\Delta\Phi$ due to the transmitted light intensity change caused by the absorption change [1, 3] are estimated to be negligibly small, i.e., in the order of 10^{-3} rad. Each $\Delta\Phi(\omega, \tau)$ and $\Delta T/T(\omega, \tau)$ spectra are the averages of 200 data runs taken for 40 s and of 20 data runs for 4 s, respectively. Here, a single data run denotes one cycle of the shutter.

Figures 5a and 6a display $\Delta T/T(\tau)$ and $\Delta\Phi(\tau)$ for H_2Pc and VOPc, respectively. They are derived simultaneously from the femtosecond frequency-domain interference spectra by Fourier transform [3]. In addition, Figs. 5b and 6b show $\Delta T/T(\tau)$ measured using the FDI apparatus with the reference beam blocked to prevent interference fringes. Figure 6b displays $\Delta T/T(\tau)$ for both parallel and perpendicular pump and probe polarizations. The decay curves of Fig. 5a and b for H_2Pc agree very well, as do the curves of Fig. 6a and b for VOPc, demonstrating the validity of simultaneous detection of both phase and transmission changes by the FDI.

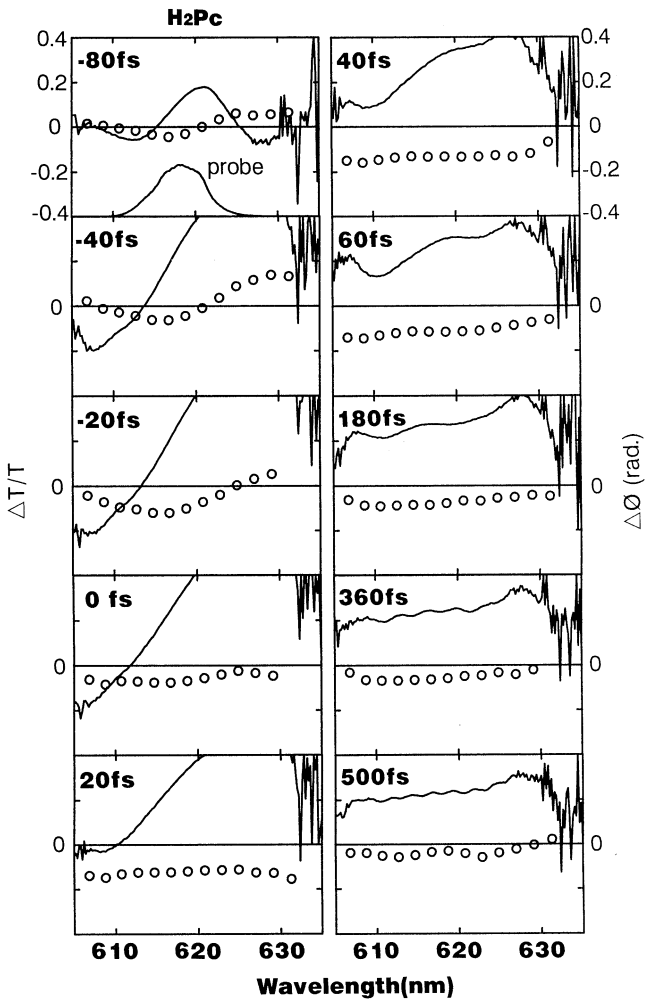

Fig. 3. $\Delta T/T(\omega, \tau)$ (*solid line*) and $\Delta\Phi(\omega, \tau)$ (*open circles*) for H_2Pc

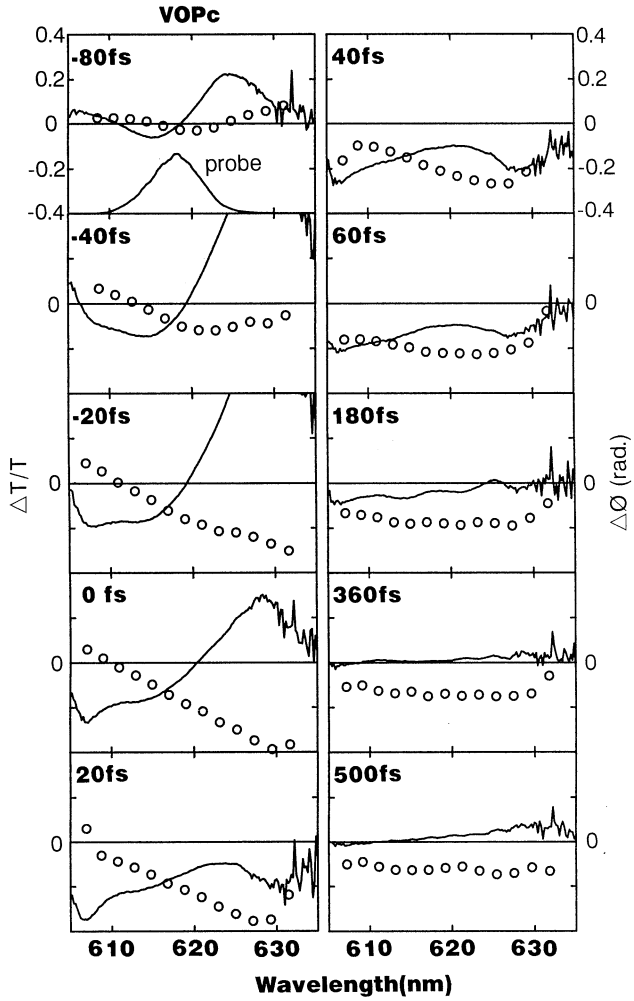

Fig. 4. $\Delta T/T(\omega, \tau)$ (*solid line*) and $\Delta\Phi(\omega, \tau)$ (*open circles*) for VOPc

3.2 Bimolecular decay

As the excitation density is estimated to exceed 10^{21} cm^{-3}, exciton–exciton annihilation (bimolecular decay) plays a major role in the decay dynamics of excitons in aromatic cycles [24] and macrocyclics [12–15, 17]. When the bimolecular decay is dominant, the exciton density, n, obeys the rate equation [12]

$$dn/dt = -\zeta t^{-1/2} n^2, \tag{1}$$

where the $t^{-1/2}$ dependence arises from annihilation via long-range dipole–dipole interaction or motion-limited diffusion [25], and ζ is the annihilation rate constant. This equation leads to

$$n/n_0 = 1/(1 + 2\zeta n_0 t^{1/2}), \tag{2}$$

where n_0 is the initial exciton density. Fitting the decay curve in Fig. 2a with this function using only one adjustable parameter, ζn_0, yields

$$\zeta n_0 = 2.3 \times 10^5 \text{ s}^{-1/2}.$$

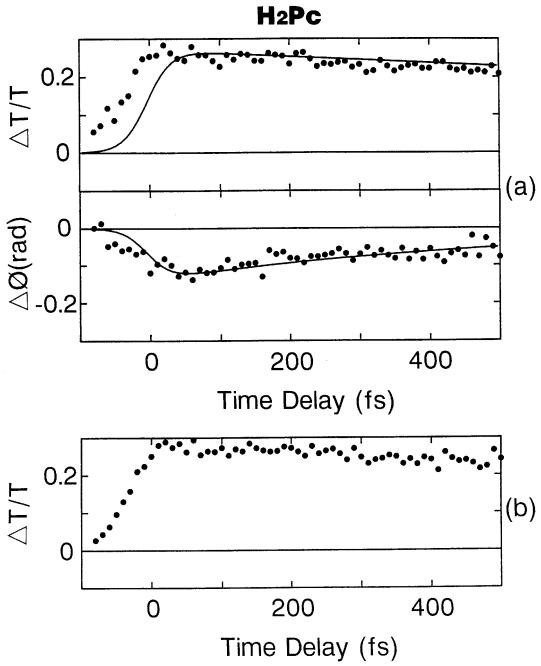

Fig. 5. **a** $\Delta T/T(\tau)$ and $\Delta\Phi(\tau)$ derived simultaneously from FDI data by Fourier analysis. **b** $\Delta T/T(\tau)$ obtained with FDI apparatus by blocking the reference beam. *Solid curves* are fitting functions in (11)

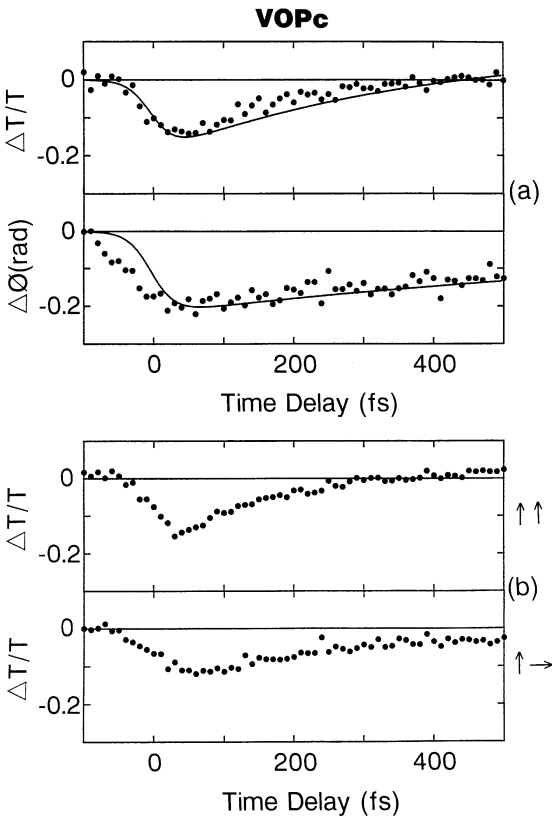

Fig. 6. **a** $\Delta T/T(\tau)$ and $\Delta\Phi(\tau)$ both calculated from FDI data by the Fourier analysis. **b** $\Delta T/T(\tau)$ obtained with FDI apparatus with the reference beam blocked for parallel and orthogonal pump and probe polarizations. *Solid curves* are fitting functions in, (12)

The value of ζ agrees with that of Greene et al. within a factor of two. Since the estimation of the exciton density is difficult in such experiments because of position-dependent density, the discrepancy may be simply due to the errors in the estimations of exciton densities in both experiments.

3.3 Different dynamics between $\Delta\Phi(\tau)$ and $\Delta T/(T\tau)$

As shown in Figs. 5a and 6a, the signs and magnitudes of the signals differ markedly between H_2Pc and VOPc in spite of the same absorbance at 620 nm. Recalling that the real and imaginary parts of $\chi^{(3)}$ correspond to $\Delta\Phi$ and $(\Delta T/T)/2$ [3], respectively, $|\mathrm{Im}\,\chi^{(3)}|$ is larger than $|\mathrm{Re}\,\chi^{(3)}|$ in H_2Pc, and vice versa in VOPc. This difference between H_2Pc and VOPc is attributed mainly to the different locations of the pump–probe wavelength in the absorption spectra. H_2Pc was pumped at the Q band peak resulting in bleaching of the peak, whereas VOPc was excited on the high energy side of the Q band. This excitation also bleaches the Q band, but induced absorption dominates the bleaching in the probed region of VOPc at early times since Pcs have a broad induced absorption band between the B and Q bands [12, 15, 17].

More important is that $\Delta\Phi(\tau)$ and $\Delta T/T(\tau)$ in VOPc show substantially different dynamics at 620 nm in Fig. 6a. Such different decay kinetics at the same wavelength were previously observed for semiconductor nanocrystallites [26] and for amorphous semiconductors [27, 28]. These results were explained in terms of multi-level contributions, i.e., both intraband and interband contributions [26] or both carrier and temperature effects [28].

Briefly, different decay dynamics between $\Delta T/T$ and $\Delta\Phi$ at the same wavelength result from excited species at different energy levels exhibiting different relaxation dynamics. They are more fully understood in terms of the pump-induced polarization change ΔP and susceptibility change $\Delta\chi$ [2, 3] for a multi-level system as follows:

$$\Delta P(t,\tau) = \sum_{ij} \chi_{ij}(t) \otimes [E_{\mathrm{pr}}(t)\ \Delta N_{ij}(t+\tau)], \tag{3}$$

$$\Delta\chi(\omega,\tau) = \sum_{ij} \chi_{ij}(\omega)\ F[E_{\mathrm{pr}}(t)\ \Delta N_{ij}(t+\tau)]/E_{\mathrm{pr}}(\omega), \tag{4}$$

where $\otimes$ denotes the convolution operation, F is the Fourier transformation, E_{pr} is the electric field of the probe, ΔN_{ij} is the change in the population difference between levels i and j, and χ_{ij} is the susceptibility contributed from the polarization between levels i and j [29]. $\Delta N_{ij}(t)$ is determined by the rate equations of the system to show a time evolution depending on i and j. For the ideal probe pulse, i.e., a δ-function pulse $E_{\mathrm{pr}}(t) = E_0\delta(t)$, (4) reduces to

$$\Delta\chi(\omega,\tau) = \sum_{ij} \chi_{ij}(\omega)\ \Delta N_{ij}(\tau) \tag{5}$$

to obtain the relations

$$\Delta T/T(\omega, \tau) \propto \sum_{ij} \mathrm{Im}\, \chi_{ij}(\omega)\ \Delta N_{ij}(\tau),$$
$$\Delta \Phi(\omega, \tau) \propto \sum_{ij} \mathrm{Re}\, \chi_{ij}(\omega)\ \Delta N_{ij}(\tau). \quad (6)$$

Since $\chi_{ij}(\omega)$ and $\Delta N_{ij}(\tau)$ are generally different for different (ij) pairs and $\mathrm{Im}\, \chi_{ij}(\omega) \neq \mathrm{Re}\, \chi_{ij}(\omega)$, $\Delta T/T(\omega, \tau)$ and $\Delta \Phi(\omega, \tau)$ exhibit different dependence on τ even at the same ω. At the same time, the $\Delta T/T(\omega, \tau)$ [or $\Delta \Phi(\omega, \tau)$] spectrum changes not only in amplitude but also in shape with time delay.

For VOPc, the positive region of the $\Delta T/T(\omega, \tau)$ spectrum expands to shorter wavelengths from 180 to 500 fs in Fig. 4. This spectral change corresponds to the substantial difference in the decay kinetics between $\Delta T/T(\tau)$ and $\Delta \Phi(\tau)$ in this time region in Fig. 6a. For H_2Pc, on the other hand, the $\Delta T/T(\omega, \tau)$ spectrum changes only slightly from 180 to 500 fs as shown in Fig. 3, consistent with the smaller decay difference between $\Delta T/T(\tau)$ and $\Delta \Phi(\tau)$ in this time region in Fig. 5a.

3.4 VOPc

From Fig. 1, femtosecond excitation at 620 nm is expected to cause 660 nm Q-band depletion in VOPc. At delays from 180 to 500 fs in Fig. 4, $\Delta T/T(\omega, \tau)$ increases with wavelength, suggesting that a bleaching peak is located at a longer wavelength than 635 nm. This is supported by our previous fs pump–probe measurements using white-light continuum probe pulses in [17], where a large absorption saturation of the Q band is observed immediately after excitation of a spin-coated film of $(t\text{-Bu})_{1.1}$VOPc dissolved in polystyrene. In Fig. 9 of [17], the dominant signal in $\Delta T/T(\omega, \tau)$ over the visible region is the absorption saturation signal peaked around 670 nm, which is expected to cause a significant negative phase change around 620 nm. Although the typical decay time of $\Delta T/T(\tau)$ at 650–700 nm in Fig. 10 of [17] is longer than that of $\Delta \Phi(\tau)$ in Fig. 6 of the present paper, if the lower excitation intensity for the former (20 GW/cm^2) than for the latter (85 GW/cm^2) is taken into account, the dynamics of $\Delta \Phi(\tau)$ in the present paper is interpreted to reflect mainly the 660 nm Q-band bleaching dynamics affected by the intensity-dependent bimolecular decay process.

In Fig. 6, the sign of the $\Delta T/T(\tau)$ changes; initial induced absorption evolves into absorption saturation in about 400 fs in such a way that the positive region of the $\Delta T/T(\omega, \tau)$ spectrum expands to shorter wavelengths from 180 to 500 fs in Fig. 4. From this behavior, there are two possible interpretations for the sign change. First, the exciton population responsible for bleaching the inhomogeneously broadened Q band diffuses spectrally as discussed in [17]. Second, the population of the initial levels corresponding to the induced absorption relaxes into lower levels, resulting in a blue shift of the induced absorption. Since the bleaching and induced absorption may overlap to some degree in the probed spectral region, we cannot determine which is the case for changing the VOPc $\Delta T/T(\omega, \tau)$ spectra.

Spectral diffusion explains the different $\Delta T/T(\tau)$ dynamics in VOPc between parallel and perpendicular pump–probe polarizations in Fig. 6b, where the parallel bleaching signal grows faster than the perpendicular signal. Here, diffusion of the population via energy transfer to sites with different energies is accompanied by a decreasing anisotropy of the susceptibility change initially induced. Since energy transfer is more efficient to a site with a smaller directional angle difference, diffusion to the perpendicular direction is delayed by the relaxation time of anisotropy. This results in a delayed rise of the perpendicular bleaching signal. This explanation is consistent with the results of previous transient spectral hole burning experiments where decay of the induced anisotropy in fluoro-aluminum Pc was directly observed [16].

3.5 H_2Pc

In contrast to the complex dynamics in VOPc, that of H_2Pc can be explained approximately in the framework of a simple two-level system, as indicated by the similar decay dynamics of $\Delta T/T(\tau)$ and $\Delta \Phi(\tau)$ in Fig. 5a. To be seen closely, however, $\Delta \Phi(\tau)$ decays faster than $\Delta T/T(\tau)$. This is clearly shown in solid fitting curves, which have decay times of 2.7 ± 0.3 ps for $\Delta T/T$ and 530 ± 60 fs for $\Delta \Phi$ as will be discussed in Sect. 4. This decay difference may also be explained in terms of spectral diffusion as follows. If the $\Delta T/T$ spectral hole broadens, the negative peak in $\Delta \Phi(\omega, \tau)$ on the short wavelength side of the hole will blue-shift. At a wavelength appropriately located between the positive $\Delta T/T$ bleaching peak and the negative $\Delta \Phi$ peak, the $\Delta \Phi$ magnitude will decay due to the blue shift of the $\Delta \Phi$ peak while the $\Delta T/T$ magnitude at that wavelength will be affected only slightly by the spectral diffusion. In fact, $\Delta T/T(\omega, \tau)$ in Fig. 3 becomes less inclined from 60 to 500 fs, suggesting spectral diffusion. Consequently, the observed dynamics in H_2Pc cannot be explained simply by a two-level system. A more complicated model, an inhomogeneously broadened system for example, is required to explain the observed dynamics in H_2Pc.

3.6 Determination of the nonlinear susceptibility

The real and imaginary parts of the nonlinear susceptibilities at 620 nm are evaluated [30] from the peak excitation intensity of 8.5×10^{10} W/cm^2 and the sample thicknesses of 0.12 μm and 0.16 μm for H_2Pc and VOPc, respectively, as $\chi^{(3)}_{\mathrm{eff}} = (-2.7 + 2.9\mathrm{i}) \times 10^{-10}$ esu for H_2Pc and $\chi^{(3)}_{\mathrm{eff}} = (-3.4 - 1.3\mathrm{i}) \times 10^{-10}$ esu for VOPc. The error is within 30% in both cases mainly caused by the spot size misestimation. The above effective values $\chi^{(3)}_{\mathrm{eff}}$'s obtained with 60 fs pulses depend on the incident pulse duration since the signals of non-instantaneous response are normalized by the pulse peak intensity.

4 Induced modulation effects

The transient spectra in Figs. 3 and 4 must be carefully interpreted because they do not indicate the intrinsic

origin. They are distorted by induced amplitude and phase modulations of the probe [18] as expressed by $F[E_{pr}(t)\ \Delta N_{ij}(t+\tau)]/E_{pr}(\omega)$ in (4), which induces the destruction of the Kramers–Kronig relations [2, 3].

Only in the two special cases, the measurement of $\Delta T(\omega, \tau)$ alone is sufficient to obtain the intrinsic spectra given by (5). First, if the probe is a δ-function pulse, $F[E_{pr}(t)\ \Delta N_{ij}(t+\tau)]/E_{pr}(\omega)$ is reduced to $\Delta N_{ij}(\tau)$. Then, $\mathrm{Re}\sum_{ij}\chi_{ij}(\omega)\ \Delta N_{ij}(\tau)$ can be deduced from the Kramers–Kronig transformation of $\Delta T/T(\omega, \tau) \propto \mathrm{Im}\sum_{ij}\chi_{ij}(\omega)\ \Delta N_{ij}(\tau)$. Second, if a two-level system is probed with a finite-duration pulse, $\Delta\chi(\omega, \tau) = \chi(\omega)\,\Delta N(\tau)$ is precisely determined from the linear susceptibility $\chi(\omega)$ and $\Delta N(\tau)$ which is deduced from deconvolution of $\Delta T/T(\tau) \propto \int \mathrm{d}\omega\,|E_{pr}(\omega)|^2 \Delta T/T(\omega, \tau) \propto \int \mathrm{d}t\,|E_{pr}(t)|^2 \Delta N(t+\tau)$ [31].

Otherwise, i.e., in the case of a multi-level system probed with a finite-duration pulse, the measurement of both $\Delta T/T(\omega, \tau) \propto \mathrm{Im}\,\Delta\chi(\omega, \tau)$ and $\Delta\Phi(\omega, \tau) \propto \mathrm{Re}\Delta\chi(\omega, \tau)$ is necessary to deduce the intrinsic dynamics as explained in the following. Since (4) can be rewritten as

$$\Delta\chi(\omega, \tau) = F[E_{pr}(t) \sum_{ij} \chi_{ij}(\omega)\ \Delta N_{ij}(t+\tau)]/E_{pr}(\omega), \tag{7}$$

the intrinsic dynamics $\sum_{ij}\chi_{ij}(\omega)\ \Delta N_{ij}(t+\tau)$ can be reproduced from the signal $\Delta\chi(\omega, \tau)$ by using the inverse Fourier transformation as

$$F^{-1}[\Delta\chi(\omega, \tau)\ E_{pr}(\omega)]/E_{pr}(t) = \sum_{ij} \chi_{ij}(\omega)\ \Delta N_{ij}(t+\tau). \tag{8}$$

For this procedure, the functions of both real and imaginary parts of $\Delta\chi(\omega, \tau)$ are needed.

For the present results, the measured spectral range is so narrow that the above procedure cannot actually be performed. Instead, the contribution of the induced modulation effects in Figs. 3 and 4 can be numerically estimated as follows. If $\chi_{ij}(\omega)$ is almost independent of frequency (χ_{ij}) in the observed spectral range as in the case of rapid dephasing or large detuning [18], then (7) is reduced to

$$\Delta\chi(\omega, \tau) \propto F\{E_{pr}(t)[-\Delta\phi(t+\tau) - i\Delta\kappa(t+\tau)]\}/E_{pr}(\omega), \tag{9}$$

where $\Delta\phi(t+\tau) \propto -\mathrm{Re}\{\sum_{ij}\chi_{ij}\Delta N_{ij}(t+\tau)\}$ and $\Delta\kappa(t+\tau) \propto -\mathrm{Im}\{\sum_{ij}\chi_{ij}\Delta N_{ij}(t+\tau)\}$. In this case, the ω dependence of $\Delta\chi(\omega, \tau)$ is only due to the modulation effects and it can be determined from the numerical simulation as in (3) of [18] or (21) of [3]. Because of the narrow spectral range for the present results, we can perform the simulation as a reasonable approximation.

For the simulation, the functions $\Delta\phi(t)$ and $\Delta\kappa(t)$ must be determined from the experimental data. For this purpose, the H_2Pc dynamics in Fig. 5a were fit to a single exponential decay to obtain decay times 2.7 ± 0.3 ps for $\Delta T/T$ and 530 ± 60 fs for $\Delta\Phi$. The value of 2.7 ps is regarded as an effective initial decay time in the bimolecular decay. For VOPc in Fig. 6a, $\Delta\Phi(\tau)$ was also fit to another single exponential decay with a decay time 900 ± 100 fs while $\Delta T/T(\tau)$ was tentatively fit to a response function

$$f(t) = A - B\exp(-t/T) \quad \text{for } t > 0 \tag{10}$$

from Fig. 2b. Since the fitting parameters $A, B,$ and T cannot be determined reliably from the short dynamics in Fig. 6, we used the data in Fig. 2b until 3 ps to obtain the values of $A = 0.53 \pm 0.01$, $B = 1.53 \pm 0.04$, and $T = 380 \pm 20$ fs.

Thus $2\Delta\kappa(t)$ ($= -\Delta T/T$) and $\Delta\phi(t)$ are expressed as follows. For H_2Pc,

$$\begin{aligned} &2\Delta\kappa(t) = CI(\tau) \otimes [\theta(t)\exp(-t/T)] \\ &\text{with } T = 3 \text{ ps and } 2\Delta\kappa(t)_{\max} = -0.26, \\ &\Delta\phi(t) = CI(\tau) \otimes [\theta(t)\exp(-t/T)] \\ &\text{with } T = 500 \text{ fs and } \Delta\phi(t)_{\max} = -0.12\,. \end{aligned} \tag{11}$$

For VOPc,

$$\begin{aligned} &2\Delta\kappa(t) = CI(t) \otimes \{\theta(t)\,[0.5 - 1.5\exp(-t/T)]\} \\ &\text{with } T = 400 \text{ fs and } 2\Delta\kappa(t)_{\max} = 0.15, \\ &\Delta\phi(t) = CI(\tau) \otimes [\theta(t)\exp(-t/T)] \\ &\text{with } T = 1 \text{ ps and } \Delta\phi(t)_{\max} = -0.2\,. \end{aligned} \tag{12}$$

Here, $I(t)$ is a squared hyperbolic secant function of 60 fs FWHM, $\theta(t)$ is the normalized step function, and C is a fitting constant determined from the maxima of $\Delta T/T$ and $\Delta\Phi$ curves in Figs. 5 and 6. The $2\Delta\kappa(t)$ and $\Delta\phi(t)$ obtained above are shown in Fig. 7, and also in Figs. 5a and 6a. Figure 6a shows that $2\Delta\kappa(t)$ does not fit the $\Delta T/T$ data very well [32], indicating that (10) is not the most appropriate function to describe the dynamics, but the following simulations are not affected qualitatively even with the simple fitting function. Also note that the fit is not good near zero delay in Figs. 5a and 6a because of the coherent coupling effects between the pump and probe: the experimental data show an earlier rise than the fitting

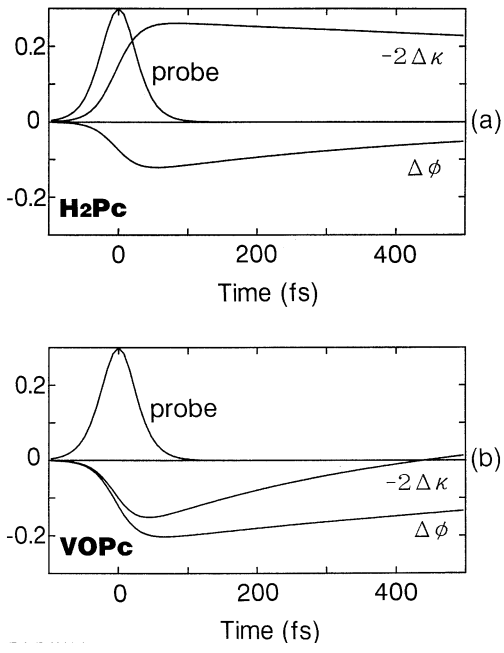

Fig. 7. Fitted time evolutions of the absorption and phase change, $-2\Delta\kappa(t)$ and $\Delta\phi(t)$ in (11) for (a) H_2Pc and in (12) for (b) VOPc

curves in Fig. 5a and $\Delta T/T(\tau)$ rises delayed from $\Delta\Phi(\tau)$ in Fig. 6a. The coherent coupling effects will be discussed in detail in Sect. 5.

To simulate the spectra in Figs. 3 and 4, the transmitted probe field with excitation is expressed by $E_{\mathrm{pr}}(t)\exp[-\Delta\kappa(t+\tau)+\mathrm{i}\Delta\phi(t+\tau)]$, which is then Fourier transformed to obtain $\Delta T/T(\omega,\tau)$ and $\Delta\Phi(\omega,\tau)$ [3, 18]. The results of the simulation are illustrated in Fig. 8. Since the rapid dephasing condition is almost satisfied [18], the induced modulation effects dominate the signals and the simulation qualitatively agrees with the experimental results.

The results in Fig. 8 can be qualitatively explained as in Sect. 4 of [18]. Assuming instantaneous response time for simplicity, the probe field is amplitude and phase modulated by the absorption and phase changes, $\Delta\kappa(t)$ *and* $\Delta\phi(t)$, respectively, and Fourier transformed (FT) to obtain $\Delta T/T(\omega,\tau)$ and $\Delta\Phi(\omega,\tau)$:

$$\begin{aligned} &E(t)\exp[\mathrm{i}\omega_0 t-\Delta\kappa(t+\tau)-\mathrm{i}\Delta\phi(t+\tau)]\\ &\quad\sim E(t)\exp(\mathrm{i}\omega_0 t)\,[1-\Delta\kappa(t+\tau)+\mathrm{i}\Delta\phi(t+\tau)]\\ &\quad\sim[E(t)-\delta_1 E(t+\tau)+\mathrm{i}\delta_2 E(t+\tau)]\exp(\mathrm{i}\omega_0 t)\\ &\quad\overset{\mathrm{FT}}{\rightarrow} E(\omega-\omega_0)\,\{1-(\delta_1-\mathrm{i}\delta_2)\exp[\mathrm{i}(\omega-\omega_0)\tau]\}, \end{aligned} \tag{13}$$

$$\begin{aligned} \Delta T/T(\omega,\tau)&\sim -2\delta_1\cos(\omega-\omega_0)\tau-2\delta_2\sin(\omega-\omega_0)\tau,\\ \Delta\Phi(\omega,\tau)&\sim\delta_2\cos(\omega-\omega_0)\tau-\delta_1\sin(\omega-\omega_0)\tau. \end{aligned} \tag{14}$$

Substituting $\delta_1<0$ and $\delta_2<0$ for H_2Pc and $\delta_1>0$ and $\delta_2<0$ for VOPc, the qualitative features of the signals can be explained by the simple expressions above.

Differences of Figs. 3 and 4 from Fig. 8 indicate the effect of $\chi_{ij}(\omega)$ spectral dependence. That is, the signs of the slopes of both $\Delta\Phi$ and $\Delta T/T$ spectra at 180 fs in Figs. 3 and 4 are opposite to those at 160 fs in Fig. 8. At these long delay times, the $\Delta\Phi(\tau)$ and $\Delta T/T(\tau)$ signals change more slowly than at near-zero delay times. As proved previously [2, 3], at such longer delays when the probe pulse experiences a nearly steady state, $\Delta T/T(\omega,\tau)$ and $\Delta\Phi(\omega,\tau)$ represent approximately an intrinsic susceptibility change given by (6). Therefore, $\Delta T/T(\omega,\tau)$ and $\Delta\Phi(\omega,\tau)$ measured at delays longer than 100 fs are considered to represent the intrinsic spectra. More precisely, the intrinsic spectra must have steeper slopes than the observed, because the observed slopes are partially compensated for by the opposite slopes of the modulated spectra in Fig. 8.

At 500 fs, $\Delta\Phi(\omega,\tau)$ in both Figs. 3 and 4 shows an oscillatory structure with an approximately 10 nm period. No such oscillations are observed in $\Delta T/T(\omega,\tau)$. At 500 fs, the reference pulse precedes the pump pulse by only 120 fs. Thus, when measuring $\Delta\Phi(\omega,\tau)$, the reference pulse is slightly disturbed by the pump pulse to yield transient oscillations [18, 33]. The artificial oscillations are not present in $\Delta T/T(\omega,\tau)$ as the reference beam is blocked for these measurements.

5 Coherent coupling effects

As mentioned previously, the rise of $\Delta T/T(\tau)$ is retarded from $\Delta\Phi(\tau)$ near zero delay in Fig. 6a. Since $\Delta\Phi(\tau)$ reflects

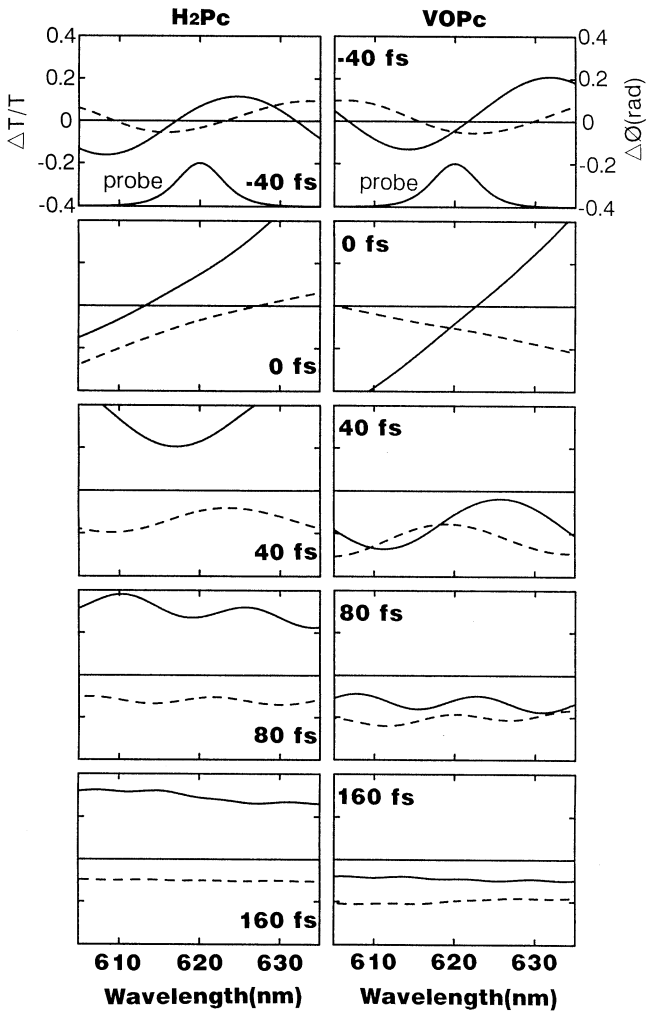

Fig. 8. $\Delta T/T(\omega,\tau)$ and $\Delta\Phi(\omega,\tau)$ due to the induced modulation effects, calculated using the functions in Fig. 7

the saturation dynamics around 660 nm as discussed in Sect. 3.4, the delayed buildup in $\Delta T/T(\tau)$ may be caused by a delay of the induced absorption with respect to the absorption saturation as observed previously for fluoroaluminum Pc thin films [15]. However, since the delay is within the pulse duration in Fig. 6, this behavior may also be caused by coherent coupling effects which distort the signals at the early delay times within the pulse duration. Under the rapid-dephasing approximation, the coherent effects consist of two terms, namely, the amplitude grating and the phase grating. It is known that if both pump and probe pulses are linearly chirped, the phase grating gives the $\Delta T/T(\tau)$ signal an antisymmetric contribution with respect to zero delay [34]. Similarly, the amplitude grating gives the $\Delta\Phi(\tau)$ signal an antisymmetric contribution as shown below. As a result, the signal intensities are reduced at negative delays and enhanced at positive delays in $\Delta T/T(\tau)$ and vice versa in $\Delta\Phi(\tau)$. These effects are derived as follows.

When both pump and probe pulses are linearly chirped with a chirp rate γ, they are expressed by

$$\begin{aligned} E_{\mathrm{ex}}(t)&=E(t)\exp(\mathrm{i}\omega t+\mathrm{i}\gamma t^2),\\ E_{\mathrm{pr}}(t)&=E(t-\tau)\exp[\mathrm{i}\omega(t-\tau)+\mathrm{i}\gamma(t-\tau)^2]. \end{aligned} \tag{15}$$

Then, the pump-induced change in the probe field including the coherent terms is expressed in terms of a complex response function $R(t) = -\mathrm{i}[R_\mathrm{r}(t) - \mathrm{i}R_\mathrm{i}(t)]$, where $R(t<0) = 0$ and its relation to $\Delta\phi(t)$ and $\Delta\kappa(t)$ in Sect. 4 is given in Appendix A, as follows:

$$\Delta E_\mathrm{pr}(t) = E_\mathrm{pr}(t)\int \mathrm{d}t'\, E^*_\mathrm{ex}(t')\, E_\mathrm{ex}(t')\, R(t-t') + E_\mathrm{ex}(t)\int \mathrm{d}t'\, E^*_\mathrm{ex}(t')\, E_\mathrm{pr}(t')\, R(t-t'), \quad (16)$$

where $*$ denotes complex conjugate. The signals with the FDI are given by

$$\Delta\phi(\tau)\propto \mathrm{Im}\, S(\tau) = I_\mathrm{r}(\tau) + S_\mathrm{r}(\tau) + A_\mathrm{i}(\tau),$$
$$\Delta K(\tau)\propto \mathrm{Re}\, S(\tau) = I_\mathrm{i}(\tau) + S_\mathrm{i}(\tau) + A_\mathrm{r}(\tau)$$
$$[\Delta T/T = 2\Delta K/\textstyle\int \mathrm{d}t\, |E_\mathrm{pr}(t)|^2], \quad (17)$$

where

$$\begin{aligned} S(\tau) &= \int \mathrm{d}t\, E^*_\mathrm{pr}(t)\, \Delta E_\mathrm{pr}(t) \\ &= \iint \mathrm{d}t\, \mathrm{d}t'\, E^2(t-\tau)\, E^2(t')\, R(t-t') \\ &\quad + \iint \mathrm{d}t\, \mathrm{d}t'\, E(t-\tau)\, E(t)\, E(t')\, E(t'-\tau) \\ &\qquad \exp[2i\gamma\tau(t-t')] R(t-t'), \end{aligned} \quad (18)$$

$$\begin{aligned} I_\mathrm{r}(\tau) &= -\iint \mathrm{d}t\, \mathrm{d}t'\, E^2(t-\tau)\, E^2(t')\, R_\mathrm{r}(t-t'), \\ S_\mathrm{r}(\tau) &= -\iint \mathrm{d}t\, \mathrm{d}t'\, F(t,t',\tau)\, R_\mathrm{r}(t-t')\cos 2\gamma\tau(t-t'), \\ A_\mathrm{r}(\tau) &= \iint \mathrm{d}t\, \mathrm{d}t'\, F(t,t',\tau)\, R_\mathrm{r}(t-t')\sin 2\gamma\tau(t-t'), \\ I_\mathrm{i}(\tau) &= -\iint \mathrm{d}t\, \mathrm{d}t'\, E^2(t-\tau)\, E^2(t')\, R_\mathrm{i}(t-t'), \\ S_\mathrm{i}(\tau) &= -\iint \mathrm{d}t\, \mathrm{d}t'\, F(t,t',\tau)\, R_\mathrm{i}(t-t')\cos 2\gamma\tau(t-t'), \\ A_\mathrm{i}(\tau) &= -\iint \mathrm{d}t\, \mathrm{d}t'\, F(t,t',\tau)\, R_\mathrm{i}(t-t')\sin 2\gamma\tau(t-t'), \\ F(t,t',\tau) &= E(t-\tau)\, E(t)\, E(t')\, E(t'-\tau). \end{aligned} \quad (19)$$

Without chirp, the coherent coupling signals have only symmetric terms $S_{\mathrm{r,i}}(\tau)$ with respect to $\tau = 0$. On the other hand, when the pump and probe pulses are both linearly chirped, there are antisymmetric terms $A_{\mathrm{r,i}}(\tau)$. The signs are determined as $I_\mathrm{r}I_\mathrm{i} \gtrless 0$ and $A_\mathrm{r}A_\mathrm{i} \lessgtr 0$ for $R_\mathrm{r}R_\mathrm{i} \gtrless 0$. Therefore, irrespective of the sign of $R_\mathrm{r}R_\mathrm{i}$, the antisymmetric terms contribute in a different manner (constructively and destructively) to the growth of $\Delta\Phi$ and ΔK resulting in the different growth behavior (steeper and slower growth). If one pulse is chirped and the other is not, the effect is similar but less pronounced for the same γ.

Previously [3] different growth behavior was observed also for CdS_xSe_{1-x}-doped glass. Figure 9 shows $\Delta T/T(\tau)$ and $\Delta\Phi(\tau)$ simultaneously obtained at 620 nm for a 2 mm thick R63 filter. $\Delta\Phi(\tau)$ is the same as that in Fig. 7 of [3]. Here $\Delta T/T(\tau)$ grows more rapidly than $\Delta\Phi(\tau)$. The growth behavior is dependent on the pulse chirp, which was varied by a four-SF11-prism sequence after an amplifier, indicating that it was caused by the coherent coupling effects. The result in Fig. 9 is qualitatively reproduced in Fig. 10 by the numerical calculation of (17) using $R_\mathrm{r}(t) = R_\mathrm{i}(t) = -\theta(t)\ \exp(-t/\tau)$, $\tau = 10$ ps, $\gamma = -10^{-4}$ fs^{-2} (negative chirp), and a hyperbolic-secant envelope for the pump and probe pulses with 60 fs FWHM. Note that a 60 fs pulse with a chirp rate $\gamma = 10^{-4}$ fs^{-2} (positive) is generated when a FT-limited 58 fs pulse is transmitted through a 4.2 mm thick BK7 glass or a 1.1 mm thick SF11 glass if a Gaussian envelope is assumed. These values of thickness are estimated using the relation between γ and

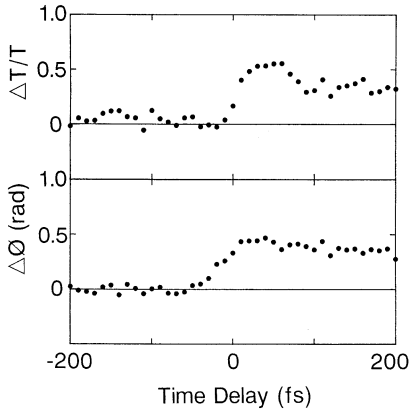

Fig. 9. $\Delta T/T(\tau)$ and $\Delta\Phi(\tau)$ for the R63 filter, obtained simultaneously by the FDI.

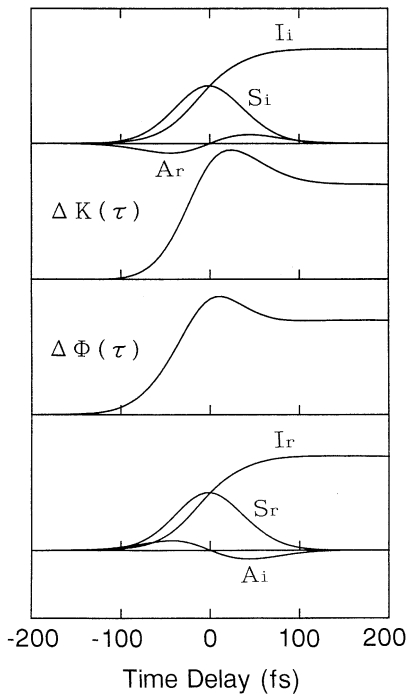

Fig. 10. Numerical calculation of (17) with $R_\mathrm{r}(t) = R_\mathrm{i}(t) = -\theta(t)\exp(-t/\tau)$, $\tau = 10$ ps, $\gamma = -10^{-4}$ fs^{-2} (negative chirp), and a hyperbolic-secant envelope for the pump and probe pulses of 60 fs FWHM.

Group Velocity Dispersion (GVD) given in Appendix B. With a prism compensator adjusted optimally (within 0.5 mm SF11 GVD), nearly FT-limited pulses were obtained before the sample insertion. Therefore the observed negative chirp with the chirp rate $\gamma < 0$, $|\gamma| > 10^{-4}$ fs^{-2}, must be brought into the pulses mostly by the GVD near resonance in the R63 filter sample, since GVD slightly below a resonance peak is negative. In fact, the $\Delta\Phi(\omega,\tau)$ spectra in Fig. 6 of [3] show a negative second derivative with respect to λ for $-\mathrm{Re}\,\Delta\chi$ ($\mathrm{Re}\,\Delta\chi < 0$), suggesting negative GVD for $\mathrm{Re}\,\chi$ around 620 nm. Since the optical density of the R63 filter is 1.0 at 620 nm, the observed negative chirp is producible as roughly estimated in Appendix C.

For VOPc, the real and imaginary parts, R_r and R_i, are both positive as deduced from $\Delta\phi < 0$ and $\Delta\kappa > 0$ in Fig. 7b and from (A4). Thus, when both pulses are down-chirped ($\gamma < 0$), the antisymmetric terms A_r and A_i cause the transmission change $\Delta T/T(\tau)$ $[\Delta K(\tau)]$ to grow more steeply and the phase change $\Delta\Phi(\tau)$ to grow more slowly, as in Fig. 6a, than in the case of no chirp. The negative chirp may be introduced by negative GVD above resonance in the VOPc sample.

For H_2Pc, the difference in the growth behavior is not as pronounced as for VOPc. This is because GVD at exact resonance is negligible, as estimated in Appendix C.

6 Conclusions

We have applied femtosecond frequency-domain interferrometry to the macrocyclic systems, H_2Pc and VOPc, and measured both real and imaginary parts of $\Delta\chi$ ($\Delta\Phi$ and $\Delta T/T$) as a function of ω and τ around 620 nm.

For both samples, $\Delta\Phi(\tau)$ and $\Delta T/T(\tau)$ show different dynamics at 620 nm. In a two-level system the dynamics of $\Delta\Phi(\tau)$ and $\Delta T/T(\tau)$ are expected to be the same, while in a multi-level or inhomogeneously broadened system they are different. The dynamical difference between $\Delta T/T(\tau)$ and $\Delta\Phi(\tau)$ is more distinct in VOPc than in H_2Pc. This is because the Q band of H_2Pc is resonant at 620 nm while that of VOPc is substantially red-shifted from 620 nm resulting in more contributions from off-resonant levels. The dynamical difference offers a criterion of the appropriateness of the two-level model. For VOPc, the phase-change dynamics at 620 nm reflects the Q-band exciton dynamics at 660 nm. That is, the phase-change data yield dynamical information for regions outside the probed spectral region.

Using both $\Delta T/T(\tau)$ and $\Delta\Phi(\tau)$, the spectral changes due to the induced amplitude and phase modulations were satisfactorily reproduced. The modulation effects cause significant distortion in transient spectra even when the pump and probe do not overlap. Because of different dynamics between $\Delta\Phi(\tau)$ and $\Delta T/T(\tau)$, the modulation effects can be ascertained only when $\Delta\Phi(\tau)$ is measured independently from $\Delta T/T(\tau)$. Since the modulation effects are unavoidable for a finite-duration probe pulse, in order to obtain true transient spectra, both $\Delta T/T$ and $\Delta\Phi$ spectra must be measured as in (8) unless the relevant system is described by a two-level system or a δ-function probe is used.

If pump and probe pulses are chirped, phase and amplitude gratings produced by the coherent coupling between the pump and probe give antisymmetric contributions to $\Delta T/T(\tau)$ and $\Delta\Phi(\tau)$ with respect to zero delay, resulting in different growth behavior between $\Delta T/T(\tau)$ and $\Delta\Phi(\tau)$. Thus, care must always be taken when interpreting near-zero delay signals.

Appendix A

Relation of $R(t)$ to $\Delta\phi(t)$ and $\Delta\kappa(t)$

The response function $R(t)$ in Sect. 5 is related to $\Delta\phi(t)$ and $\Delta\kappa(t)$ in Sect. 4 as follows. With the pump-induced complex refractive index change in a material, $\Delta n_c(t) = \Delta n(t) - i\Delta k(t)$, the change in the probe field is expressed as

$$\begin{aligned} &E_{pr}(t) + \Delta E_{pr}(t) \\ &\quad = E_0(t)\exp\{i\omega[t - \Delta n_c(t)\,L/c]\} \\ &\quad \sim E_0(t)\exp(i\omega t)\,[1 + i\Delta\phi(t) - \Delta\kappa(t)] \end{aligned} \tag{A1}$$

and

$$\Delta E_{pr}(t)\,[\propto -i\Delta P(t)] = E_{pr}(t)\,[i\Delta\phi(t) - \Delta\kappa(t)], \tag{A2}$$

where $\Delta\phi(t) = -\Delta n(t)\,\omega L/c$, $\Delta\kappa(t) = \Delta k(t)\,\omega L/c$, L is the material thickness, c is the velocity of light, and $\Delta P(t)$ is the induced polarization change. The signals caused by the incoherent terms are given by

$$\begin{aligned} &\Delta\Phi \propto \mathrm{Im}\int \mathrm{d}t\, E^*_{pr}(t)\,\Delta E_{pr}(t) = \int \mathrm{d}t\,|E_{pr}(t)|^2\Delta\phi(t), \\ &\Delta K \propto \mathrm{Re}\int \mathrm{d}t\, E^*_{pr}(t)\,\Delta E_{pr}(t) = -\int \mathrm{d}t\,|E_{pr}(t)|^2\Delta\kappa(t), \end{aligned} \tag{A3}$$

where

$$\begin{aligned} &\Delta\phi(t) = -\int \mathrm{d}t'\,|E_{ex}(t')|^2 R_r(t - t'), \\ &\Delta\kappa(t) = \int \mathrm{d}t'\,|E_{ex}(t')|^2 R_i(t - t'). \end{aligned} \tag{A4}$$

Appendix B

Relation between a chirp rate γ and GVD

A chirped pulse with a Gaussian envelope is formulated as

$$E(\omega) = E_0\pi^{1/2}\exp(-\tau_p^2\omega^2/4 - i\rho\omega^2/4), \tag{B1}$$

$$\mathrm{E}(t) = F^{-1}[E(\omega)] = E_0(\varepsilon - i\gamma)^{1/2}\exp(-\varepsilon t^2 + i\gamma t^2). \tag{B2}$$

Here

$\varepsilon = \tau_p^2/(\tau_p^4 + \rho^2)$, $\gamma = \rho/(\tau_p^4 + \rho^2)$, $[\tau_p^2 = \varepsilon/(\gamma^2 + \varepsilon^2)$, $\rho = \gamma/(\gamma^2 + \varepsilon^2)]$, and

$$\rho = 2D_{gv}L, \tag{B3}$$

where D_{gv} is the expression of GVD given by

$$D_{gv} = (\lambda^3/2\pi c^2)(\mathrm{d}^2n/\mathrm{d}\lambda^2). \tag{B4}$$

When the FWHM of $|E(t)|^2$ is 60 fs, ε is obtained from $1/\varepsilon = 60^2/(2\ln 2)$. Using $\lambda\,\mathrm{d}^2n/\mathrm{d}\lambda^2 = 0.11\ \mu\mathrm{m}^{-1}$ for BK7 and $0.42\ \mu\mathrm{m}^{-1}$ for SF11 at 620 nm [35], the thicknesses L given in Sect. 5 are estimated.

Appendix C

GVD near resonance

GVD near an absorption peak is estimated as follows. The complex refractive index $n_c = n - ik$ is related with the linear susceptibility $\chi = \chi_r - i\chi_i$ as

$$n_c = (1 + 4\pi\chi)^{1/2} \sim 1 + 2\pi\chi \quad \text{when } |\chi| \ll 1. \tag{C1}$$

then

$$n = 1 + 2\pi\chi_r \quad \text{and} \quad k = 2\pi\chi_i . \tag{C2}$$

$\chi(\omega)$ is given by

$$\chi_r(\omega) = A(\Omega - \omega)\,/[(\Omega - \omega)^2 + \Gamma^2] \tag{C3}$$

and

$$\chi_i(\omega) = A\Gamma/[(\Omega - \omega)^2 + \Gamma^2], \tag{C4}$$

where Ω is a transition frequency, Γ is a phase relaxation rate, and A is an appropriate coefficient. Then, using (B4), (C2), and (C3),

$$D_{gv} = (4\pi A/C)\,[\Omega(\Omega - \omega)^3 + 3\Gamma^2\omega(\Omega - \omega) - \Gamma^4]/ \\ [(\Omega - \omega)^2 + \Gamma^2]^3. \tag{C5}$$

If the optical density (OD) = 2 at the absorption peak ($\omega = \Omega$), $T_2 = 1/\Gamma = 30$ fs, and $2\pi c/\Omega = 620$ nm,

$$-\log_{10}[\exp(-2k\Omega L/c)] = 2 \quad \text{and} \quad k = 2\pi\chi_i(\Omega) = 2\pi A/\Gamma. \tag{C6}$$

Just on resonance at $\omega = \Omega$,

$$D_{gv} = -(4\pi A/c)\,(1/\Gamma^2). \tag{C7}$$

Then, from (B3), (C6), and (C7) we obtain $\rho = 2D_{gv}L = -4\ln 10/(\Omega\Gamma) = -9.1 \times 10\ \text{fs}^2$. This corresponds to a negligibly small chirp rate $\gamma = -1.5 \times 10^{-5}\ \text{fs}^{-2}$ for a FT-limited 58 fs Gaussian pulse. Therefore the GVD in the H_2Pc sample should not cause an appreciable difference in the rising behavior between $\Delta T/T$ and $\Delta\Phi$.

At $\omega = \Omega - \Gamma$ (slightly below the resonance peak, where OD ~ 1),

$$D_{gv} = (4\pi A/c)\,(\Gamma - \Omega)/4\Gamma^3 \sim -(\pi A/c)\Omega/\Gamma^3 \quad (\Omega \gg \Gamma). \tag{C8}$$

Then, from (C6) and (C8) we obtain $\rho = 2D_{gv}L = -\ln 10/\Gamma^2 = -2.1 \times 10^3\ \text{fs}^2$. This gives $\gamma = -2.0 \times 10^{-4}\ \text{fs}^{-2}$ for a FT-limited 58 fs Gaussian pulse. Therefore the GVD in the R63 filter should cause significant negative chirp.

In fact, the oscillator strength of the Q band in phthalocyanines is so large that χ is an order of 1 in (C1). Therefore the approximation in (C1) is not valid for the H_2Pc and VOPc samples. However, we verified by numerical calculation that the precise calculation gives a similar value for ρ. This is because the effects of the large χ are only a blue shift of the absorption peak from $\omega = \Omega$ and slight distortion in the shape of $n_c(\omega)$ from that of $\chi(\omega)$.

References

1. E. Tokunaga, A. Terasaki, T. Kobayashi: Opt. Lett. **17**, 1131 (1992)
2. E. Tokunaga, A. Terasaki, T. Kobayashi: Phys. Rev. A **47**, R4581 (1993)
3. E. Tokunaga, A. Terasaki, T. Kobayashi: J. Opt. Soc. Am. B **12**, 753 (1995)
4. E. Tokunaga, A. Terasaki, T. Kobayashi: J. Opt. Soc. Am. B **13**, (1996) (in press)
5. C.C. Leznoff, A.B.P. Lever (eds.) : *Phthalocyanines*: *Properties and Applications* (VCH, New York 1989)
6. D. Dolphin (ed.) : *The Porphyrins* (Academic, New York 1978)
7. T. Wada, Y. Matsuoka, K. Shigehara, A. Yamada, A.F. Garito, H. Sasabe: In *Photoresponsive Materials*, Proc. Materials Research Society Int'l Meeting on Advanced Materials (Materials Research Society, Pittsburgh, PA 1989) Vol. 12, p. 75
8. M. Hosoda, T. Wada, A. Yamada, A.F. Garito, H. Sasabe: Jpn. J. Appl. Phys. **30**, L1486 (1991); **30**, 1715 (1991)
9. J.W. Wu, J.R. Heflin, R.A. Norwood, K.Y. Wong, O. Zamani-Khamiri, A.F. Garito, P. Kalyanaraman, J. Sounik: J. Opt. Soc. Am. B **6**, 707 (1989)
10. A. Grund, A. Kaltbeitzel, A. Mathy, R. Schwarz, C. Bubeck, P. Vermehren, M. Hanack: J. Phys. Chem. **96**, 7450 (1992)
11. H. Hoshi, K. Kohama, S. Fang, Y. Maruyama: Appl. Phys. Lett. **62**, 3080 (1993)
12. B.I. Greene, R.R. Millard: Phys. Rev. Lett. **55**, 1331 (1985)
    B.I. Greene, R.R. Millard: J. Phys. (Paris), **46**, C7-371 (1985)
13. Z.Z. Ho, N. Peyghambarian: Chem. Phys. Lett. **148**, 107 (1988)
14. M.K. Casstevens, M. Samoc, J. Pfleger, P.N. Prasad: J. Chem. Phys. **92**, 2019 (1990).
15. V.S. Williams, S. Mazumdar, N.R. Armstrong, Z.Z. Ho, N. Peyghambarian: J. Phys. Chem. **96**, 4500 (1992).
16. V.S. Williams, J.P. Sokoloff, Z.Z. Ho, C. Arbour, N.R. Armstrong, N. Peyghambarian: Chem. Phys. Lett. **193**, 317 (1992).
17. A. Terasaki, M. Hosoda, T. Wada, H. Tada, A. Koma, A. Yamada, H. Sasabe, A.F. Garito, T. Kobayashi: J. Phys. Chem. **96**, 10534 (1992)
18. E. Tokunaga, A. Terasaki, T. Wada, K. Tsunetomo, Y. Osaka, T. Kobayashi: J. Opt. Soc. Am. B **10**, 2364 (1993)
19. J.H. Sharp, M. Lardon: J. Phys. Chem. **72**, 3230 (1968)
20. C.H. Griffiths, M.S. Walker, P. Goldstein: Mol. Cryst. Liq. Cryst. **33**, 149 (1976).
21. T.-H. Huang, J.H. Sharp: Chem. Phys. **65**, 205 (1982)
22. M. Kasha, H.R. Rawls, M.A. El-Bayoumi: Pure Appl. Chem. **11**, 371 (1965)
23. N. Kobayashi, A.B.P. Lever: J. Am. Chem. Soc. **109**, 7433 (1987)
24. T. Kobayashi, S. Nagakura: Mol. Phys. **24**, 695 (1972)
25. R.C. Powell, R.G. Kepler: Phys. Rev. Lett. **22**, 636 (1969); **22** 1232 (1969)
    R.C. Powell, Z.G. Soos: J. Lumin. **11**, 1 (1975)
26. D. Cotter, C.N. Ironside, B.J. Ainslie, H.P. Girdlestone: Opt. Lett. **14**, 317 (1989)
27. J. Kuhl, E.O. Gobel, Th. Pfeiffer, A. Jonietz: Appl. Phys. A **34**, 105 (1984)
28. C. Tanguy, D. Hulin, A. Mourchid, P.M. Fauchet, S. Wagner: Appl. Phys. Lett. **53**, 880 (1988)
    P.M. Fauchet, D. Hulin: J. Opt. Soc. Am. B **6**, 1024 (1989)
    P.M. Fauchet, A. Mourchid, D. Hulin, C. Tanguy, R. Vanderhaghen: J. Non-Cryst. Solids **114**, 564 (1989)
29. In (3) and (4), the coherent coupling contribution between the pump and probe pulses is not taken into account for simplicity
30. P.N. Butcher, D. Cotter: *The Elements of Nonlinear Optics* (Cambridge Univ. Press, Cambridge 1990) p. 306
31. This relation is evident from Appendix B of [3]
32. As far as the 500 fs dynamics is concerned, $A = 0.16$, $B = 1.16$, and $T = 172$ fs give the best fit to the data in Fig. 6b, but substantial deviation for longer delay times than 500 fs
33. B. Fluegel, N. Peyghambarian, G. Olbright, M. Lindberg, S.W. Koch, M. Joffre, D. Hulin, A. Migus, A. Antonetti: Phys. Rev. Lett. **59**, 2588 (1987)
    C.H. Brito-Cruz, J.P. Gordon, P.C. Becker, R.L. Fork, C.V. Shank: IEEE J. QE-**24**, 261 (1988)
    M. Lindberg, S.W. Koch: Phys. Rev. B **38**, 7607 (1988)
    J.P. Sokoloff, M. Joffre, B. Fluegel, D. Hulin, M. Lindberg, S.W. Koch, A. Migus, A. Antonetti, N. Peyghambarian: Phys. Rev. B **38**, 7615 (1988)
    M. Joffre, D. Hulin, A. Migus, A. Antonetti: J. Mod. Opt. **35**, 1951 (1988)
34. T.F. Heinz, S.L. Palfrey, K.B. Eisenthal: Opt. Lett. **9**, 359 (1984)
    S.L. Palfrey, T.F. Heinz: J. Opt. Soc. Am. B **2**, 674 (1985)
35. Z. Bor, B. Racz: Appl. Opt. **24**, 3440 (1985)